Journal of the Korean Society
for Nondestructive Testing
Vol. 25, No. 6 (2005. 12)

Fabrication of Microcantilever Ultrasound Sensor and Its Application to the Scanning Laser Source Technique

Younghoon Sohn*,† and Sridhar Krishnaswamy*

Abstract The scanning laser source (SLS) technique has been proposed recently as an effective way to investigate small surface-breaking defects. By monitoring the amplitude and frequency changes of the ultrasound generated as the SLS scans over a defect, the SLS technique has provided enhanced signal-to-noise performance compared to the traditional pitch-catch or pulse-echo ultrasonic methods. An extension of the SLS approach to map defects in microdevices is proposed by bringing both the generator and the receiver to the near-field scattering region of the defects. To facilitate near-field ultrasound measurement, silicon microcantilever probes are fabricated using microfabrication technique and their acoustical characteristics are investigated. Then, both the laser-generated ultrasonic source and the microcantilever probe are used to monitor near-field scattering by a surface-breaking defect.

Keywords: microcantilever probe, microfabrication, ultrasound sensor, near-field scanning laser source

1. Introduction

In recent work at Northwestern University, it has been shown that near-field scattering of ultrasound generated by a scanning laser source (SLS) can be used to effectively identify surface flaws in macro-scale structures (Kromine et al., 2000, Sohn and Krishnaswamy, 2002, Sohn and Krishnaswamy, 2004). In the SLS technique, the scanning laser ultrasound source was in the near-field of a scatterer, and an optical or piezoelectric detector was used to measure the ultrasound in the far-field. It was noted that distinct variations are observed in the far-field signals as the SLS scans past surface-breaking flaws. These changes were attributed to the near-field scatterer redirecting parts of the ultrasonic beam (which might otherwise have gone into the bulk of the object) towards the far-field detector. As the source approaches the defect, the amplitude and frequency of the detected signal significantly increase. This increase is readily detectable compared to weak echoes from the flaw in a standard pulse-echo method. The variation in the signal is due to interaction of the direct ultrasonic wave with the waves scattered by a defect in the near-field of the source and changes in the conditions of generation of ultrasound when the SLS is in the vicinity of the defect.

In this paper, an extension of the SLS technique to the case of near-field scattering and near-field detection is proposed. The basic idea is to put both the source and the receiver in the near-field of a scatterer and to monitor changes in the received signal as both the source and the receiver scan over flaws. The intended applications of this approach include detection of

Received: October 7, 2005, Accepted: November 22, 2005. * Center for Quality Engineering and Failure Prevention, Northwestern University, 2137 Tech Drive, Evanston, IL 60208 3020, USA, † Corresponding author: y-sohn@northwestern.edu

flaws in micro-scale components such as microelectronic packages where space constraints necessitate very compact measurement devices. For the purpose of near-field measurement of ultrasound especially on optically non-reflective surfaces, a contact ultrasound detector is fabricated using silicon microfabrication techniques. The ultrasound receiver is composed of a microcantilever, a probe tip, and a handling body, similar to commercially available atomic force microscope (AFM) probes. Commercial AFM probes, however, are not suitable in view of their relatively low frequency response (a few hundred kilohertz) when compared to the ultrasonic frequencies of interest to this work. We have therefore designed and microfabricated these receivers. In this paper, first the fabrication and the vibration characteristics of microcantilevers are discussed. We demonstrate that a suitably designed cantilever detector can perform as a resonance ultrasound detector. We then describe how such a resonant detector can be used in conjunction with the SLS technique for detection of flaws.

2. Fabrication of Microcantilever Ultrasound Receiver

Several types of microcantilever scanning probes have been reported in the literatures (Albrecht et al., 1990, Rosner et al., 2002). Depending on the intended application, the scanning probe which is composed of the cantilever and a contacting tip, should meet several criteria: (1) a low flexural stiffness of the cantilever (2) a high resonant frequency, (3) a high mechanical quality (Q) factor, (4) high lateral stiffness to avoid twisting, (5) incorporation of a mirror-like optical reflector to monitor the cantilever deflection, and (6) a sharp or high aspect ratio probe tip. The combined requirements of a low stiffness and a high resonant frequency can be met by reducing the mass of the cantilever. Thus microfabrication techniques offer advantages for producing cantilevers with good mechanical properties. The fundamental resonant frequency of AFM cantilevers which are commercially available ranges from 30 to 300 kHz. In noncontacting AFM experiment, increasing the Q factor increases the sensitivity of measurements, however, the Q factor is of less importance in contacting mode. In fact, bringing the cantilever into contact with the sample surface causes significant resonance changes. High lateral stiffness in the cantilever is desirable to reduce the effects of lateral forces. However in some other applications, especially dynamic application of scanning probe, the lateral response of the cantilever can be an indication for surface stiffness measurement. For high-resolution ultrasonic force microscopy (UFM) measurements, a sharp probe tip should necessarily be formed at the end of the cantilever (Yamanaka and Ogiso, 1994). However, depending on the application, blunt tips may be applicable. In this work on near-field scanning laser source (NF-SLS) technique, very high spatial resolution is not needed, but the cantilever needs to have much higher fundamental frequencies than those of commercial probes. This can be obtained by choosing an appropriate geometry for the cantilever.

The fabrication of microcantilever and probe tip uses surface micromachining to deposit and pattern dielectric and metal thin-films, and bulk micromachining for three-dimensional probe structure definition. Conventional microfabrication techniques have been used for constructing pyramidal tips, rectangular cantilever beams and chip bodies. The fabrication processes are similar to the AFM probe fabrication processes (Albrecht et al., 1990, Rosner et al., 2002, Kovacs, 1998). The processes combine existing batch fabrication techniques for microfabricating thin-film cantilevers on silicon substrate with methods of producing integrated tips. Three photomasks were designed to create cantilevers, tips, and chip body as shown in Fig. 1. Photomask #1 has the tip caps which are rectangular shapes and tip

protection structures. These protection structures work as tip protector during the next processes, for instance photoresist spinning and reactive ion etching (RIE). Photomask #2 creates cantilevers and chip bodies along with the supporting bars which hold the chip bodies after back side releasing. Photomask #3 has the opening pattern from the back side of substrate and compensation structures at the convex corners (Sandmaier et al., 1991) of the chip bodies. The photomasks have an alignment pattern for the alignment of the various patterns. The cantilevers, tips, and chip bodies are made of double-side polished, n-doped silicon wafers with 1-100Ω-cm resistivity, 3 inch diameter, 350μm thickness and (100) crystal orientation. The major layouts in the fabrication process are: (1) defining the tips and cantilevers by RIE and (2) releasing the backside of the wafer to define the chip bodies by anisotropic potassium hydroxide KOH etching. Masks were designed for batch fabrication of 96 chips in a 3-inch wafer. A chip module has a rectangular cantilever of 50μm (100μm) width × 200μm (400μm) length × 15μm thickness, a probe tip of ~ 0.15μm radius × ~ 10μm height, and a chip body of 1.5 mm width × 3.5 mm length. Fabrication processes are presented in Fig. 2 in detail.

1. The silicon wafer is cleaned using H_2O_2 (30%) and H_2SO_4 (96%) mixture at a ratio of 3:1 (Piranha clean). SiO_2 is then deposited on the front side using plasma enhanced chemical vapor deposition (PECVD) at 300℃, 650mTorr using 800sccm of SiH_4 and 355sccm N_2O mixture. 30 minutes deposition time and 20W plasma power produces 830nm thickness of silicon oxide thin-film.

2. SiO_2 is patterned for the rectangular tip caps which will determine the base size of the pyramidal tip. The other oxide area of the tip caps is selectively removed by buffered hydrofluoric acid (BHF 6:1). The photoresist is left on the caps and the exposed Si is etched

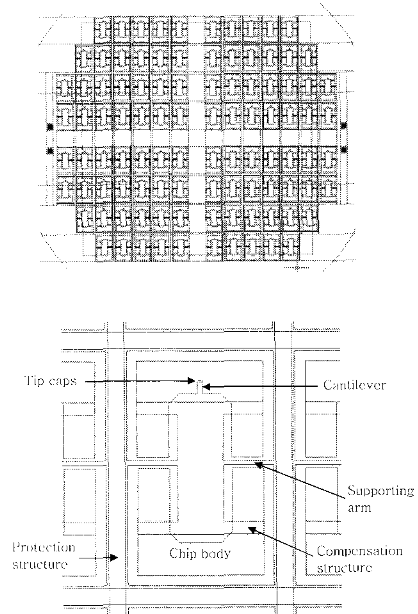

Fig. 1 Three photomasks are designed for batch fabrication of 96 chips in a 3 inch wafer. Each mask includes tip caps, cantilevers, chip bodies, supporting arms, protection, and compensation structures.

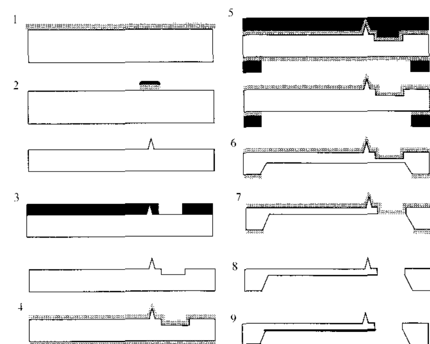

Fig. 2 Fabrication processes: (1) PECVD SiO_2 on front side; (2) definition of tip by RIE, (3) definition of cantilever and chip body by RIE, (4) LPCVD Si_3N_4 on both sides, (5) opening of Si_3N_4, (6) KOH etch for the body releasing on back side, (7) complete releasing by RIE, (8) removing Si_3N_4, (9) evaporation of Al thin film on back side.

using isotropic RIE (SF_6) to create non-vertical side walls. The presence of photoresist on top of the SiO_2 caps enhances the anisotropy of the etching which yields rather steep sidewalls (Albrecht et al., 1990). Etching is closely controlled until the pyramids are about 10 μm high. The RIE results in silicon pyramids with concave sides remaining SiO_2 caps on top of the tips. Because the etching rate is not sufficiently uniform over the whole 3 inch wafer surface, the tip height and radius are different from the center to edge of the wafer. The remaining SiO_2 caps are removed by BOE after removing remaining photoresist. At this point, the probe tips have been formed.

3. For the protection of fabricated tips during the subsequent photo-lithography process, thick photoresist is coated using low spinning speed and several additional deposition processes are done. After the thick photoresist is patterned with relatively long exposure time, the cantilevers and chip bodies are defined using RIE. Also the etching is closely monitored until the cantilever thickness is about 15 μm. To remove the remaining photoresist Piranha clean process is performed for a sufficient time.

4. The deposition of 530nm thick low-stress Si_3N_4 film on both wafer sides is performed using low-pressure chemical vapor deposition (LPCVD).

5. The front side of the wafer on which the tip and cantilever structures are established is then protected from mechanical ablation by coating thick photoresist at low spinning speed and then hard baking at 135℃ for 45minutes. The Si_3N_4 on the bottom side is patterned using CF_4 in RIE and the remaining photoresist is removed on both sides by Piranha clean.

6. To define each of the chip bodies, an anisotropic potassium hydroxide (KOH) etch is used. A 45% KOH solution at 90℃ etches at a rate of 1.3 μm/min. The etching process is closely monitored and stopped when the remaining Si thickness is about 20 μm.

7. Next, the cantilevers are released using RIE (SF_6). Only the backside of the wafer is etched until only the support bars and the nitride layer is holding the chip bodies on the front side. After this final silicon etching step, the cantilevers are 11~19 μm thick. The protective nitride on the front side and patterned nitride on the back side are removed by 85% phosphoric acid at boiling temperature (157℃) at the etching rate of ~300nm/hour.

8. A 50 nm layer of Al is evaporated on the backside of the released chips to enhance optical reflectance of the cantilevers.

In Fig. 3, scanning electron microscopy (SEM) images show one of the results of the fabrication among the various sizes of chip modules. During the process, some of the tips were under etched producing blunt tip radius (~50nm sharp, ~250nm blunt) and some of cantilevers were produced with thickness ranging from 11 μm to 19 μm. This is because the RIE process did not provide uniform etching rates across the whole wafer area during the etching process. Also the side walls of the cantilever are not exactly perpendicular to the top plane of the cantilever due to the isotropic etching of RIE. However, as demonstrated next, the blunt tip radii obtained provides more than adequate resolution for our purposes, and the cantilevers with the higher thicknesses were suitable as ultrasound receivers into the MHz range.

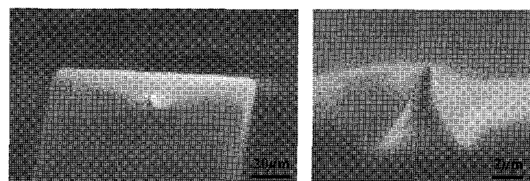

Fig. 3 SEM images of fabricated cantilever and tip

3. SLS Application with Microcantilever Ultrasound Sensor

3.1 Fundamental frequency of free cantilever vibration

The fundamental frequencies of flexural mode of cantilevers with homogeneous cross section, such as rectangular ones can be calculated using (Thomson and Dahleh, 1998)

$$f_n = \frac{(k_n L)^2}{2\pi} \sqrt{\frac{E}{12\rho}} \cdot \left(\frac{d}{L^2}\right) \quad (1)$$

where E is Young's modulus (E=169 GPa for <110> direction of silicon, (Wortman and Evans, 1965)), ρ is the mass density (ρ=2330 kg/m^3), d is the thickness, L is the length of the cantilever. k_n is wave number of nth order (n=1, 2, 3, ⋯) vibration mode. The coefficients k_nL with k_1L= 1.875, k_2L=4.694, k_3L=7.855 correspond to the vibration modes in the boundary configuration of clamped-free condition. The calculated frequencies for a cantilever with 200 μm length are f_1 = 0.65 MHz, f_2 = 4.09 MHz, and f_3 = 11.46 MHz for d =19 μm.

The free vibrations of microfabricated cantilever were examined experimentally. A broadband contact PZT-transducer is attached to a thick aluminum block and the body chip is attached on the opposite side using a standard couplant. The transducer generates tone burst longitudinal wave in a spectral range of 0.5 MHz to 2.5 MHz. The generated wave is transmitted into the chip body through the Al block and excites the cantilever (200 μm × 50 μm × 19 μm). The amplitude of the cantilever is measured by a stabilized Michelson interferometer using He-Ne laser (633 nm wavelength) and the beam is focused onto the end of the cantilever using a microscope video camera. Fig. 4 shows the normalized peak to peak amplitude and energy (as this is a resonant device with relatively high Q resulting in long ringing, the energy was calculated within a preselected fixed time window) versus various excited frequencies. At 0.70 MHz excitation, the amplitude and energy show the maximum values representing the fundamental frequency of the cantilever. The measured fundamental frequency is 0.76 MHz showing slight difference with the theoretical one calculated as 0.65 MHz above. The discrepancy can be attributed to the fact that the geometry of the cantilever is not a perfect rectangular shape and the clamped boundary condition is an approximation as well.

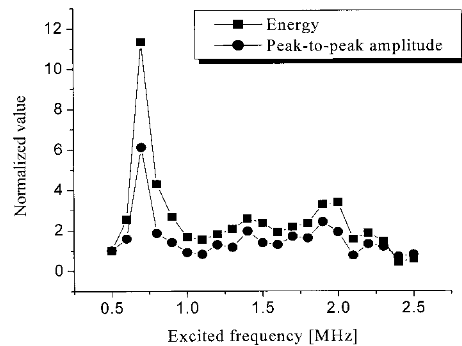

Fig. 4 Normalized energy and peak-to-peak amplitude versus excitation frequency. The energy was calculated within a preselected fixed time window.

3.2 Resonance shift of contacting cantilever

We next examined the ultrasonic response of the cantilever when the tip is in contact with a sample surface. When the cantilever tip is contacting the sample surface, out-of-plane ultrasound displacements excite the cantilever via the probe tip. The examination was performed with the setup shown schematically in Fig. 5. A tone burst (5 cycles) longitudinal wave is generated by the transducer in the spectral range of 0.5 MHz to 2.5 MHz. The sample (50 mm thick aluminum block) is attached to a micro-translation stage for control of the contact distance between the sample surface and the

receiver probe tip. Normalized values of the peak-to-peak amplitude at various excited frequencies are shown in Fig. 6. The resonant frequency of the contacting cantilever appears to change about 1.3 ~ 1.5 MHz. This is attributable to the fact that the contacting cantilever tip no longer represents a free boundary condition, but can be represented by a contact spring to model the tip-sample interaction (Rabe et al., 1996). The resonance frequencies are slightly different with each separate experiment ranging from 1.3 MHz to 1.5 MHz. The inconsistency of the frequency shift is because the cantilever force is slightly different with each experiment due to the limited accuracy of the micro-stage (~1 μm sensitivity) that is used to move the cantilever into contact with the specimen.

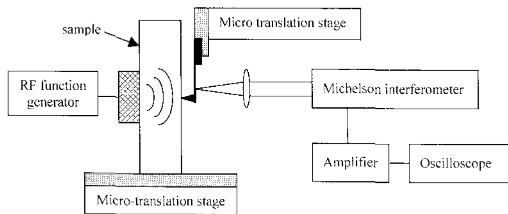

Fig. 5 Experimental setup to measure contacting cantilever vibration

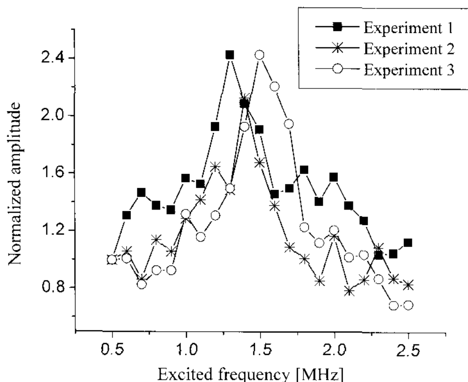

Fig. 6 Normalized amplitude versus various excitation frequencies

3.3 Near-field generation and detection of ultrasound

The resonant nature of the microcantilever ultrasound receiver and the fact that the ultrasound generated by a scanning laser source as it sweeps past a surface-breaking crack increases dramatically in frequency suggest a unique way for detecting surface-breaking defects. The basic idea is to adjust the SLS spot size so that the center frequency of the surface acoustic wave generated in regions with no defects is lower than that of the resonance frequency of the cantilever. The received signal will therefore be in general weak. Now as the SLS scans over a defect, the frequency of the generated ultrasound increases and at some point hits the resonant frequency of the receiver, resulting in a very large increase in the detected signal.

The experimental setup and typical source/receiver positions are illustrated in Fig. 7. Broadband surface acoustic wave (SAW) was generated using a *Q*-switched Nd:YAG laser (1064 nm) on an aluminum specimen which has a surface-breaking EDM notch of 2.5 mm depth and 0.3 mm width. The laser source energy was kept low enough to avoid damaging the sample surface. The source and cantilever receiver were kept close enough to each other to be within near-field region of the generated SAW (within a full wavelength of the generated SAW). Keeping the distance between the source and the cantilever receiver constant, the specimen was moved for point-by-point scanning. The diameter of the laser source (full width at half maximum assuming the distribution of laser beam is Gaussian) was adjusted by a focusing lens to be approximately 1mm on the sample surface. The frequency of the SAW generated by the laser source in regions with no flaws was measured as 0.9 MHz and the corresponding wavelength is 3.2mm. The cantilever resonance frequency was about 1.5 MHz in this case. The distance between the center of the laser source and the cantilever tip

was kept as 1.5 mm which is thoroughly shorter than the SAW wavelength. The normalized energy and peak-to-peak amplitude versus SLS positions are shown in the Fig. 8. The SLS position is defined as the distance between the first scanning position of the source and next scanning positions. From the spectrum at position A, we note that the fundamental frequency of the contacting cantilever is about 1.5 MHz because the spectrum shows peaks at both 0.9 MHz excitation frequency and 1.5 MHz resonant frequency. As the source approaches the defect, the signal amplitude detected increases (position B). One of the characteristic features of the SLS technique is that the SAW frequency component changes as the source is close to the defect because the effective source width is reduced by the edge of the defect (Kromine et al., 2000). The increase of the generated SAW frequency means that it approaches the fundamental frequency of the contacting cantilever, and therefore increases the cantilever resonant response. From the spectrum at the position B we can see that energy of the cantilever at the position B shows its maximum around the fundamental frequency of the cantilever. At position C, the receiver and the source are separated by the defect resulting in almost zero amplitude and energy detected. At position D the cantilever receiver is located just beside the defect wall detecting the increased amplitude of ultrasound due to the constructive near-field scattering by the defect. In this position, the frequency is again 0.9 MHz because the source is now far from the defect and therefore has the original full width. The energy of the cantilever vibration is increased by the constructive scattering but not as much as in position B because the frequency of scattered wave (0.9 MHz) is not the resonance frequency of the cantilever (1.5 MHz). As the receiver/source passes over the defect the amplitude and energy are the same as for position A.

The above method indicates that SLS can be combined with a resonant receiver to effectively detect surface-breaking flaws. For the detection of even smaller defects than the ones reported here, it is necessary to further increase the ultrasonic frequencies. This will necessitate either the use of even thicker micro-cantilevers with higher fundamental resonance frequencies, or the use of higher-order modes of the cantilevers already developed.

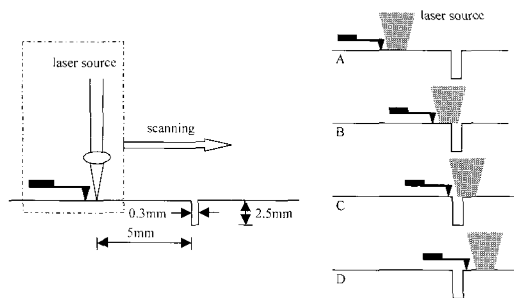

Fig. 7 Setup for the near-field SLS and typical source/receiver positions

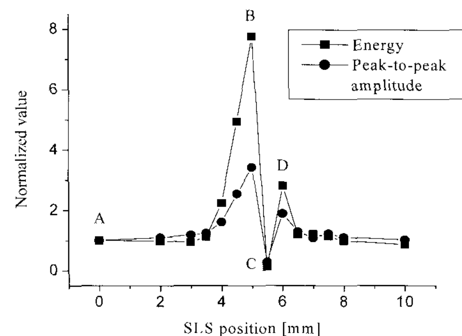

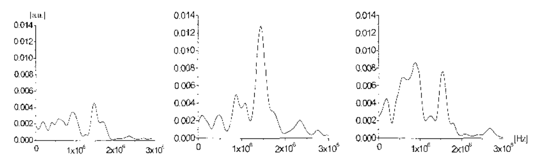

Fig 8 Normalized energy and peak-to-peak values versus SLS position. Spectrum signatures for position A, B and D.

4. Conclusion

The salient points of this paper are:

- For the purpose of near-field ultrasound measurement, a microfabricated ultrasound detector which is composed of a silicon microcantilever and a probe tip was developed. The free vibration of cantilever was investigated both analytically and experimentally.
- The performance of the fabricated microcantilever as a resonant ultrasound detector was investigated and the fundamental frequency shift of contacting cantilever was examined.
- A near-field extension to the SLS is proposed for detection of surface-breaking defects. A preliminary experiment indicates that by using a SLS whose nominal SAW frequency is set to be below the resonant frequency of a nearby microcantilever receiver, it is possible to monitor the presence of small defects as the SAW frequency shifts upwards upon scanning over a surface-breaking defect.

References

Albrecht, T.R., Akamine, S., Carver, T.E. and Quate, C.F. (1990) Microfabrication of cantilever styli for the atomic force microscope, Journal of Vacuum Science and Technology A, Vol. 8, No. 4, pp. 3386-3396.

Kovacs, G.T.A., Micromachined Transducers Sourcebook, McGraw-Hill, 1998.

Kromine, A.K., Fomitchov, P.A., Krishnaswamy, S. and Achenbach, J.D. (2000) Laser ultrasonic detection of surface breaking discontinuities: Scanning laser source technique, Material Evaluation, Vol. 58, No. 2, pp. 173-177.

Rabe, U., Janser, K. and Arnold, W. (1996) Vibrations of free and surface-coupled atomic force microscope cantilevers: Theory and experiment, Review of Scientific Instruments, Vol. 67, No. 9, pp. 3281-3293.

Rosner, B.T., Bork, T., Agrawal, V., van der Weide, D.W. (2002) Microfabricated silicon coaxial field sensors for near-field scanning optical and microwave microscopy, Sensors and Actuators A, Vol. 102, pp.185-194.

Sandmaier, H., Offereins, H.L., Kuhl, K. and Lang, W. (1991) Corner compensation techniques in anisotropic etching of (100)-silicon using aqueous KOH, in Proceedings of Transducers'91, the 6th International Conference on Solid-State Sensors and Actuators, San Francisco, CA, pp. 456-459.

Sohn, Y. and Krishnaswamy, S. (2002) Mass spring lattice modeling of the scanning laser source technique, Ultrasonics, Vol. 39, pp. 543-551.

Sohn, Y. and Krishnaswamy, S. (2004) Interaction of a scanning laser-generated ultrasonic line source with a surface-breaking flaw, Journal of Acoustic Society of America, Vol. 115, No. 1, pp. 172-181.

Thomson, W.T. and Dahleh, M.D. (1998) Theory of Vibration with Applications, Prentice Hall.

Wortman, J.J. and Evans, R.A. (1965) Young's modulus, shear modulus, and Poisson's ratio in silicon and germanium, Journal of Applied Physics, Vol. 36, No. 1, pp. 153-156.

Yamanaka, K. and Ogiso, H. (1994) Ultrasonic force microscopy for nanometer resolution subsurface imaging, Applied Physics Letter, Vol. 64, No. 2, pp. 178-180.